Acta Crystallographica Section D
Biological Crystallography
ISSN 0907-4449

Structural basis of the substrate specificity of *Bacillus cereus* adenosine phosphorylase

Paola Dessanti,[a,b]‡ Yang Zhang,[a] Simone Allegrini,[b] Maria Grazia Tozzi,[c] Francesco Sgarrella[b] and Steven E. Ealick[a]*

[a]Department of Chemistry and Chemical Biology, Cornell University, Ithaca, NY 14853-1301, USA, [b]Dipartimento di Scienze del Farmaco, Università di Sassari, Italy, and [c]Dipartimento di Fisiologia e Biochimica, Università di Pisa, Italy

‡ Present address: European Institute of Oncology, Via Adamello 16, 20139 Milan, Italy.

Correspondence e-mail: see3@cornell.edu

Received 28 October 2011
Accepted 7 January 2012

PDB References: AdoP–SO_4, 3uav; AdoP–Ado–SO_4, 3uaw; AdoP–Ino–SO_4, 3uax; D204N–Ado–SO_4, 3uay; D204N–Ino–SO_4, 3uaz.

Purine nucleoside phosphorylases catalyze the phosphorolytic cleavage of the glycosidic bond of purine (2′-deoxy)nucleosides, generating the corresponding free base and (2′-deoxy)-ribose 1-phosphate. Two classes of PNPs have been identified: homotrimers specific for 6-oxopurines and homohexamers that accept both 6-oxopurines and 6-aminopurines. *Bacillus cereus* adenosine phosphorylase (AdoP) is a hexameric PNP; however, it is highly specific for 6-aminopurines. To investigate the structural basis for the unique substrate specificity of AdoP, the active-site mutant D204N was prepared and kinetically characterized and the structures of the wild-type protein and the D204N mutant complexed with adenosine and sulfate or with inosine and sulfate were determined at high resolution (1.2–1.4 Å). AdoP interacts directly with the preferred substrate through a hydrogen-bond donation from the catalytically important residue Asp204 to N7 of the purine base. Comparison with *Escherichia coli* PNP revealed a more optimal orientation of Asp204 towards N7 of adenosine and a more closed active site. When inosine is bound, two water molecules are interposed between Asp204 and the N7 and O6 atoms of the nucleoside, thus allowing the enzyme to find alternative but less efficient ways to stabilize the transition state. The mutation of Asp204 to asparagine led to a significant decrease in catalytic efficiency for adenosine without affecting the efficiency of inosine cleavage.

1. Introduction

Purine nucleoside phosphorylases (PNPs; EC 2.4.2.1) catalyze the reversible phosphorolysis of purine (2′-deoxy)nucleosides, generating the corresponding purine base and (2′-deoxy)ribose 1-phosphate. PNPs play a key role in nucleotide metabolism, in which phosphorolysis of the N-glycosidic bond allows the purine nucleobase to be salvaged for nucleotide biosynthesis *via* phosphoribosyltransferase reactions, thus allowing energy savings with respect to *de novo* purine biosynthesis. Ribose 1-phosphate can either be utilized in the *de novo* or salvage pathways, *via* conversion to 5-phosphoribosyl 1-pyrophosphate, or can be used as a source of energy through the formation of intermediates that can enter the glycolysis and the citric acid cycle either directly or *via* the pentose phosphate pathway (Bzowska *et al.*, 2000; Tozzi *et al.*, 2006).

PNPs are members of the NP-I family of nucleoside phosphorylases, which share a common α/β-subunit fold (Pugmire & Ealick, 2002). On the basis of substrate specificity, molecular mass, subunit composition and amino-acid sequence, PNPs can be further divided into two subfamilies consisting of

homotrimers or homohexamers. Trimeric PNPs are generally specific for 6-oxopurines and have been found in eukaryotes and some prokaryotes. Hexameric PNPs are characterized by broad substrate specificity, accepting both 6-oxopurine and 6-aminopurine nucleosides, and are mainly found in prokaryotes, but have also been found in some eukaryotic parasites. The hexameric PNPs from *Thermus thermophilus* (Tahirov *et al.*, 2004) and *Plasmodium falciparum* (Daddona *et al.*, 1986) are exceptions because they do not accept adenosine as a substrate.

Bacillus cereus expresses two PNPs: one is specific for 6-oxopurines (Gardner & Kornberg, 1967) and the other is specific for 6-aminopurines (Sgarrella *et al.*, 2007). The latter enzyme is the focus of this work and is referred to as adenosine phosphorylase (AdoP). *B. cereus* AdoP is a constitutive enzyme (Tozzi *et al.*, 1981). Previous work has reported that, together with the constitutive enzyme 5′-nucleotidase, it is involved in the utilization of the sugar moiety of exogenous AMP, adenosine and inosine as an energy source. Formation of adenine causes the induction of adenosine deaminase, thus acting as a signal to the cells that adenine nucleosides are available as an energy source (Tozzi *et al.*, 1981). A specific adenosine phosphorylase activity, distinct from the inosine-guanosine phosphorylase activity, has also been detected in other members of the genus *Bacillus* (Senesi *et al.*, 1977). AdoP has been purified and characterized from *B. subtilis* (Jensen, 1978; Senesi *et al.*, 1976). AdoP from *B. cereus* is 100% identical to AdoP from *B. anthracis*, the causative agent of anthrax and a well known bioterrorism agent (Atlas, 1998). *B. anthracis* is genetically and phenotypically related to *B. cereus* (Ivanova *et al.*, 2003; Read *et al.*, 2003). Other organisms in which a distinct adenosine phosphorylase has been identified are *Schistosoma mansoni* (Miech *et al.*, 1975), *Acholeplasma laidlawii* (McElwain *et al.*, 1988), *Helix pomatia* (Trembacz & Jezewska, 1993) and *Fasciola hepatica* (Trembacz & Jezewska, 1998).

While *B. cereus* AdoP accepts both 6-aminopurine and 6-oxopurine nucleoside substrates, kinetic studies revealed a 100-fold preference (k_{cat}/K_M) for adenosine over inosine (Sgarrella *et al.*, 2007). The enzyme has a molecular weight of 164 kDa for the hexamer and 29.1 kDa for the protomer, with high sequence identity (>45%) compared with other hexameric PNPs. Structures of *B. anthracis* AdoP (Grenha *et al.*, 2005) and *B. cereus* AdoP (PDB entry 2ac7; A. Rinaldo-Matthis, S. Allegrini & F. Sgarrella, unpublished work) have previously been reported.

To investigate the structural basis of the peculiar substrate specificity of *B. cereus* AdoP, we constructed, purified and characterized the active-site mutant D204N. While the efficiency for adenosine was reduced, that for inosine increased slightly, effectively reversing the substrate specificity. We determined several crystal structures, including those of wild-type *B. cereus* AdoP, its complexes with either adenosine and sulfate or inosine and sulfate, and the D204N mutant complexed with either adenosine and sulfate or inosine and sulfate. The crystals diffracted to high resolution ranging from 1.2 to 1.4 Å. Correlation between structural data and kinetic measurements provides insights into the unique substrate preferences of *B. cereus* AdoP.

2. Experimental procedures

2.1. Site-directed mutagenesis

Site-directed mutagenesis was performed on the *B. cereus* AdoP gene cloned in pET5b vector (Novagen; F. Sgarrella, private communication), referred to in the following as pET5b/AdoP. A modification of the two-stage PCR method described by Ekici *et al.* (1997) was employed to prepare the D204N mutant. A sense mutagenic primer was designed on the sequence of the AdoP gene, starting at base 601 and containing the triplet encoding the desired mutation (in bold): 5′-ACAGTAAGT**AAT**CACATCTTCACT-3′. The sense and antisense specific primers 5′-TGCAGAA**CATATG**AGTGTA-CATATTGAAGC-3′ and 5′-CTT**GAATT**CTTATTGTTGA-ATTGCTGCATC-3′ were the same as used for the cloning of the AdoP gene and included *Nde*I and *Eco*RI restriction sites, respectively (in bold). In the first polymerase chain reaction (PCR), a 25 µl mixture consisting of 30 pmol sense mutagenic primer, 15 pmol antisense specific primer, 15 ng pET5b/AdoP DNA template, 200 µ*M* of each dNTP, 1 m*M* $MgSO_4$ and 1.25 U Platinum *Pfx* DNA polymerase (Invitrogen) in 1× PCR buffer was incubated at 367 K for 2 min; 30 consecutive cycles were then performed, each consisting of denaturation at 367 K for 30 s, annealing at 325 K for 30 s and extension at 341 K for 30 s, followed by a final incubation at 341 K for 90 s. The megaprimer obtained in this reaction was purified from agarose gel and used as an antisense primer in a second PCR reaction together with 60 pmol sense specific primer, 15 ng pET5b/AdoP, 200 µ*M* of each dNTP, 1 m*M* $MgSO_4$ and 1.25 U Platinum *Pfx* DNA polymerase in 50 µl 1× PCR buffer. The PCR conditions were the same as those used in the first PCR reaction, with 1 min of extension in each cycle. The purified mutant gene was cloned in pCRII-TOPO (Invitrogen) and then digested with *Nde*I and *Eco*RI endonucleases, and finally ligated in pET5b vector that had previously been digested with the same restriction enzymes. The resulting recombinant plasmid, designated pET5b/D204N, was sequenced on both strands at Genelab ENEA Casaccia, S. M. di Galeria (Rome, Italy) to confirm the presence of the mutation.

2.2. Expression and purification

The wild-type and mutant proteins were overexpressed in *Escherichia coli* BL21 (DE3) and purified to homogeneity using a modification of the protocol described by Sgarrella *et al.* (2007). The cells were grown at 310 K and induced with 0.4 m*M* isopropyl β-D-1-thiogalactopyranoside for 3 h after they reached an OD_{600} of 0.6. The cells were harvested by centrifugation at 5000*g* for 8 min at 277 K, after which the cell pellet was resuspended in 50 m*M* Tris–HCl pH 7.5 and lysed using a Vibra-Cell VC-400 Ultrasonic Processor (Sonics & Materials). Cell debris was removed by centrifugation at 31 000*g* for 45 min at 277 K. The crude extract was subjected to ammonium sulfate fractionation (between 46.2 and 77%

Table 1
Data-collection statistics.

Values in parentheses are for the highest resolution shell.

	AdoP–SO_4	AdoP–Ado–SO_4	AdoP–Ino–SO_4	D204N–Ado–SO_4	D204N–Ino–SO_4
Beamline	24-ID-C	23-BM	24-ID-C	24-ID-C	8-BM
Wavelength (Å)	0.97580	0.99997	0.97946	0.97946	0.97949
Space group	$P6_322$	$P6_322$	$P6_322$	$P6_322$	$P6_322$
Unit-cell parameters (Å)					
$a = b$	122.0	121.0	122.8	122.2	122.7
c	68.0	67.1	68.1	68.2	68.0
Resolution range (Å)	50.0–1.4 (1.45–1.40)	50.0–1.2 (1.24–1.20)	50.0–1.2 (1.24–1.20)	50.0–1.4 (1.45–1.40)	20.0–1.4 (1.45–1.40)
Total No. of reflections	301266	1160800	295688	415665	485298
No. of unique reflections	58855 (5791)	88363 (7949)	88185 (7217)	58861 (5806)	59410 (5858)
Multiplicity	5.1 (5.0)	13.1 (5.4)	3.4 (2.0)	7.1 (7.1)	8.2 (8.0)
Completeness (%)	99.8 (100)	97.9 (89.3)	93.5 (77.8)	99.2 (100)	99.7 (100)
$R_{\rm merge}$† (%)	5.3 (47.0)	5.2 (54.6)	6.0 (35.7)	5.6 (43.0)	7.7 (52.6)
$\langle I/\sigma(I)\rangle$	28.6 (3.0)	46.4 (2.3)	17.2 (2.2)	33.9 (5.8)	37.0 (4.8)

† $R_{\rm merge} = \sum_{hkl}\sum_i |I_i(hkl) - \langle I(hkl)\rangle| / \sum_{hkl}\sum_i I_i(hkl)$, where $\langle I(hkl)\rangle$ is the mean intensity of the i reflections with intensities $I_i(hkl)$ and common indices hkl.

saturation). The precipitate obtained was resuspended in 50 m*M* Tris–HCl pH 7.5 and further purified using a Sephacryl S300 HR column (Amersham Biosciences; 1.6 × 95 cm) pre-equilibrated with 50 m*M* Tris–HCl pH 7.5. The fractions containing the enzymatic activity were pooled together and loaded onto an N^6-adenosyl agarose affinity column (1.5 × 2.3 cm). N^6-Adenosyl agarose was prepared by dephosphorylation of 5′-AMP-agarose (Sigma) with bovine cytosolic 5′-nucleotidase II (Allegrini *et al.*, 1997). The column was washed with 0.3 *M* NaCl in 50 m*M* Tris–HCl pH 7.5. The wild-type enzyme was eluted with 10 m*M* adenosine and 0.3 *M* NaCl in 50 m*M* Tris–HCl pH 7.5. For the D204N mutant, 10 m*M* inosine replaced the adenosine in the elution buffer. The purified proteins were dialyzed against 50 m*M* Tris–HCl pH 7.5 using a 10 kDa molecular-weight cutoff cellulose membrane (Sigma).

During purification, protein concentration was measured by the Bradford assay (Bradford, 1976), while the purified AdoP concentration was determined by measuring the absorbance at 205 nm [Scopes, 1974; ε(1 mg ml^{-1}) = 29.161, calculated for the D204N mutant]. The enzymatic activity of recombinant AdoP was detected spectrophotometrically. The synthesis of adenosine from 88 µ*M* adenine and 90 µ*M* ribose 1-phosphate in 50 m*M* Tris–HCl pH 7.5 was monitored at 265 nm ($\Delta\varepsilon$ = 6.39 mM^{-1} cm^{-1}) in a coupled assay using 0.6 U ml^{-1} adenosine deaminase (Miech *et al.*, 1975). Inosine phosphorylase activity was measured at 293 nm ($\Delta\varepsilon$ = 11.26 mM^{-1} cm^{-1}) in a coupled assay using 1 m*M* inosine, 100 m*M* NaH_2PO_4/Na_2HPO_4 buffer pH 7.5 and 0.1 U ml^{-1} xanthine oxidase (Kalckar, 1947). All enzymatic assays were performed at 310 K.

2.3. Determination of kinetic parameters

Phosphorolytic activity towards adenosine and inosine was measured as described by Sgarrella *et al.* (2007). Continuous spectrophotometrical assays were performed at 310 K using an excess of phosphate (100 m*M* NaH_2PO_4/Na_2HPO_4 buffer pH 7.5) in 500 µl reaction mixtures. Adenosine phosphorolysis was measured directly at 256.5 nm ($\Delta\varepsilon$ = 1.812 mM^{-1} cm^{-1}) at 12 different concentrations of adenosine ranging from 7 to 175 µ*M* using 3.13 mU ml^{-1} D204N mutant or 3.74 mU ml^{-1} wild-type AdoP. Inosine phosphorylase activity was measured at 293 nm ($\Delta\varepsilon$ = 11.26 mM^{-1} cm^{-1}) with a coupled assay using 0.1 U ml^{-1} xanthine oxidase, 2.88 mU ml^{-1} D204N mutant or 7.76 mU ml^{-1} wild-type AdoP and 12 different inosine concentrations varying from 13 µ*M* to 1 m*M* (Sgarrella *et al.*, 2007). The kinetic parameters were analyzed by nonlinear regression data fitted to the Michaelis–Menten equation.

2.4. Crystallization

Proteins were concentrated to ∼9 mg ml^{-1} in 10 m*M* Tris–HCl pH 7.5 by ultrafiltration. Crystallization experiments were performed at 291 K using the hanging-drop vapor-diffusion method, with the drop consisting of 1.5 µl protein solution plus 1.5 µl reservoir solution and equilibrated against 400 µl reservoir solution. The optimal crystallization conditions were 1.3–1.5 *M* ammonium sulfate for the wild-type enzyme and 1.1–1.25 *M* sodium citrate pH 5.2–5.5 for the D204N mutant. Despite the different crystallization conditions, the wild type and the D204N mutant shared the same crystal morphology. Doubly terminated hexagonal crystals grew in about 4 d to typical dimensions of 150 × 150 × 200 µm. These crystals belonged to space group $P6_322$ (average unit-cell parameters a = 122, c = 68 Å), with one protomer per asymmetric unit and a Matthews coefficient (Matthews, 1968) of 2.8 Å^3 Da^{-1}, which corresponds to a solvent content of 57%.

Complexes of the wild-type protein and the D204N mutant with ligands were obtained by soaking experiments. The stabilization solutions were similar to the mother liquor except 7–15% more concentrated. Owing to crystal fragility, gradual soaking was often necessary and the ligands adenosine (Ado) or inosine (Ino) were increased in five steps to final concentrations of 1 and 10 m*M*, respectively. For D204N complexes, 7–14 m*M* ammonium sulfate was also added to the soaking solution. Soaking for 1 h was sufficient for the ligands to bind.

Prior to freezing, the crystals were cryoprotected by the addition of 18–20%(*v*/*v*) glycerol to the mother liquor or the

Table 2
Refinement statistics.

	AdoP–SO_4	AdoP–Ado–SO_4	AdoP–Ino–SO_4	D204N–Ado–SO_4	D204N–Ino–SO_4
PDB code	3uav	3uaw	3uax	3uay	3uaz
Resolution (Å)	1.4	1.2	1.2	1.4	1.4
R_{work}†	0.149	0.125	0.128	0.137	0.140
R_{free}‡	0.163	0.141	0.148	0.152	0.155
R.m.s.d. bond lengths (Å)	0.009	0.013	0.008	0.009	0.009
R.m.s.d. bond angles (°)	1.282	1.348	1.292	1.299	1.316
R.m.s.d. *B*, main chain/side chain (Å^2)	1.4/2.9	0.7/1.3	0.8/1.4	1.3/2.9	1.4/2.9
Average *B* factors (Å^2)					
Main chain/side chain	16.9/22.5	12.8/15.4	12.4/15.4	13.6/18.5	14.6/18.8
Nucleoside	—	10.3	12.0	10.4	13.9
Sulfate	18.6	10.1	10.9	12.0	14.8
Solvent	30.7	27.1	28.8	28.4	28.4
No. of protein atoms	1731	1747	1699	1756	1755
No. of water molecules	182	204	218	207	195
Ramachandran plot (%)					
Most favored regions	91.0	92.7	91.9	92.7	91.3
Additionally allowed regions	9.0	7.3	8.1	7.3	8.7

† $R_{work} = \sum_{hkl} ||F_{obs}| - |F_{calc}|| / \sum_{hkl} |F_{obs}|$, where F_{obs} and F_{calc} are observed and calculated structure factors, respectively. ‡ For R_{free} the sum extends over a subset of reflections (5%) that were excluded from all stages of refinement.

soaking solution. Crystals were frozen by quickly plunging them into liquid nitrogen.

2.5. Data collection and processing

Data sets were collected on beamlines 23-BM (MAR 225 detector), 8-BM (Quantum 315 detector) and 24-ID-C (Quantum 315 detector) at the Advanced Photon Source (APS). A total of 30–60° of data were collected from each crystal with an oscillation range of 0.5°. Data were processed using *HKL*-2000 (Otwinowski & Minor, 1997). Data-processing statistics are shown in Table 1.

2.6. Structure determination and refinement

Wild-type and D204N mutant AdoP structures were determined by molecular replacement using the *CNS* software package (Brünger *et al.*, 1998). A protomer of the *E. coli* PNP structure (PDB entry 1ecp; Mao *et al.*, 1997) was used as the search model in the absence of a better homology structure at the time. The initial rigid-body refinement and simulated annealing resulted in a model with an *R* factor of 37%. Based on a composite OMIT map, the protein backbone required minor changes and the side chains were manually adjusted using the graphics programs *O* (Jones *et al.*, 1991) and *Coot* (Emsley *et al.*, 2010). The structures were refined by alternating cycles of simulated-annealing, energy-minimization and *B*-factor refinement using *CNS* and manual rebuilding. All of the complexes showed clear $F_o - F_c$ difference density for the ligands, which were directly built into each of the structures. Solvent molecules were added after ligand building and refined by energy minimization as well as temperature-factor refinement. The water molecules were validated by checking the distance and geometry of the hydrogen bonds. In each structure, 10–13% of the residues were built in alternate conformations. The N-terminal methionine is missing in all of the structures, while residues 207–217 and 232–234 exhibited varying degrees of disorder. In the AdoP–SO_4 and AdoP–Ino–SO_4 complexes, residues 208–213 were not built in the model, while in the other structures this region was built with temperature factors above average values. The final rounds of refinement were performed using *PHENIX* (Adams *et al.*, 2011). All structures were refined to R_{work} and R_{free} values of below 15% and 17%, respectively, at which point the AdoP–Ado–SO_4 and AdoP–Ino–SO_4 complexes, both at 1.2 Å resolution, were further subjected to anisotropic refinement and converged with final R_{work}/R_{free} values of 12.5%/14.1% and of 12.8%/14.8%, respectively. More than 90% of the residues were in the most favored regions of the Ramachandran plot for all of the structures and no residues were in the disallowed region. Refinement statistics are shown in Table 2. Figures were created using *MolScript* (Kraulis, 1991), *Raster3D* (Merritt & Bacon, 1997) and *PyMOL* (DeLano, 2002).

3. Results

3.1. Kinetics of the D204N mutant

The D204N mutant was prepared to assess the contribution of Asp204 to catalysis and binding of the substrates in *B. cereus* AdoP. Asp204 is conserved in hexameric PNPs, but in trimeric PNPs it is replaced by asparagine (Asn243 in human PNP), which is essential for the phosphorolysis of 6-oxopurines (Erion, Stoeckler *et al.*, 1997; Erion, Takabayashi *et al.*, 1997). Table 3 shows the kinetic parameters determined for wild-type *B. cereus* AdoP and the D204N mutant with adenosine and inosine as substrates. Mutating Asp204 to asparagine resulted in a 420-fold decrease in k_{cat} towards adenosine, while K_m was not altered significantly. The D204N mutant showed a threefold lower K_m towards inosine, with a k_{cat} similar to that of the wild-type enzyme, resulting in a 2.2-fold increase in catalytic efficiency (k_{cat}/K_m). The overall effect of the mutation on the kinetic properties of *B. cereus* AdoP was a remarkable decrease in catalytic efficiency towards adenosine and a 1000-fold change in substrate preference; while the wild-type enzyme prefers adenosine over inosine 100-fold, the D204N mutant exhibits a ninefold preference for inosine over adenosine.

3.2. Overall structure of *B. cereus* AdoP

The overall structure of *B. cereus* AdoP is similar to those of *E. coli* PNP (Mao *et al.*, 1997) and other hexameric PNPs (Appleby *et al.*, 2001; Grenha *et al.*, 2005; Schnick *et al.*, 2005;

Table 3
Kinetic parameters of wild-type and D204N mutant AdoP with adenosine and inosine as substrates.

	K_m (μ*M*)	k_{cat} (s^{-1})	k_{cat}/K_m (s^{-1} M^{-1})
Wild type			
Adenosine	23 ± 6	75 ± 5	3.1×10^6
Inosine	315 ± 52	9.3 ± 0.5	3.0×10^4
D204N			
Adenosine	24 ± 7	0.18 ± 0.01	7.3×10^3
Inosine	102 ± 11	6.8 ± 0.2	6.6×10^4

Shi *et al.*, 2004; Tahirov *et al.*, 2004; Zang *et al.*, 2005). It should be noted that the space group of *B. cereus* AdoP in our studies was determined to be $P6_322$ with one protomer per asymmetric unit, while the deposited structure (PDB entry 2ac7) was reported to have the same unit-cell parameters but in space group $P6_3$ with two protomers per asymmetric unit. A check of the deposited data using *phenix.xtriage* (Zwart *et al.*, 2005*a*,*b*) showed a strong twofold axis with an R_{merge} of 3.3%, suggesting that the correct space group for PDB entry 2ac7 is also $P6_322$. The *B. cereus* AdoP hexamer is disc-shaped, with dimensions of approximately 100 × 100 × 36 Å (Fig. 1). The hexamer has 32 symmetry and can be thought of as a trimer of dimers (*AB*, *CD* and *EF*). Each dimer contains a pair of twofold-related active sites. The dimers are joined by *B*–*C*, *D*–*E* and *F*–*A* interfaces, which are far away from the active sites. Extensive contacts at the *B*–*C*, *D*–*E* and *F*–*A* interfaces involve α_3, α_5, β_6, β_7 and the loop between α_3 and α_4. Contacts at the *A*–*B*, *C*–*D* and *E*–*F* interfaces involve helix α_2 and loops β_2–β_3 and β_7–α_5. In most hexameric PNPs the interface containing the active site (*A*–*B* type) buries a larger surface area (Schnick *et al.*, 2005; Tahirov *et al.*, 2004); however, in *B. cereus* AdoP the dimer (*A*–*B* type) buries ∼2800 Å^2 of surface area, while the second interface (*B*–*C* type) buries ∼3500 Å^2 of surface area. The *B. cereus* AdoP protomer has the characteristic NP-I fold (Pugmire & Ealick, 2002) consisting of a single α/β-domain with a central nine-stranded β-sheet forming a distorted β-barrel that is surrounded by seven α-helices (Fig. 2).

3.3. AdoP active site

The active site was characterized using four complexes: (i) wild-type AdoP with adenosine and sulfate (AdoP–Ado–SO_4), (ii) wild type with inosine and sulfate (AdoP–Ino–SO_4), (iii) D204N with adenosine and sulfate (D204N–Ado–SO_4) and (iv) D204N with inosine and sulfate (D204N–Ino–SO_4). The active site is located at the C-terminal end of the β-barrel and can be divided into three regions: the phosphate-binding site, the ribose-binding site and the base-binding site (Fig. 3). The phosphate-binding and ribose-binding sites are identical in all of our AdoP structures, while important differences occur in the base-binding site depending on the substrate.

The phosphate-binding site is occupied by a sulfate ion in all of the complexes, as widely used in the determination of both trimeric and hexameric PNP since it shares similar chemical properties with the phosphate ion and is an inhibitor of the phosphorolysis reaction (Appleby *et al.*, 2001; Mao *et al.*, 1997; Tahirov *et al.*, 2004). Gly20, Arg87, Thr90 and Arg43* (where the asterisk indicates a residue from the adjacent subunit) make hydrogen bonds to the sulfate O atoms. The sulfate ion also donates hydrogen bonds to the ribose O3′ and O2′. In the binary complex, two water molecules replace the ribose O atoms.

In the ribose-binding site, the 5′-hydroxyl group of the sugar hydrogen-bonds to His4* and a water molecule. Met180 is involved in a hydrophobic interaction with the hydrophobic

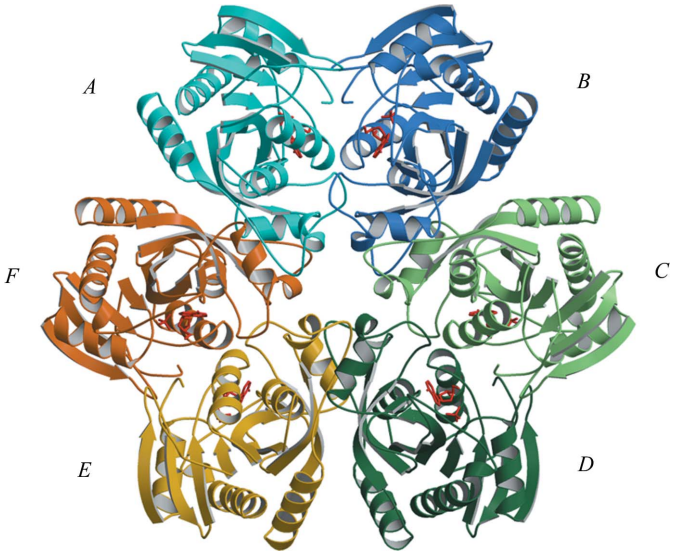

Figure 1
Structure of the *B. cereus* AdoP hexamer in ribbon representation. Protomers *B*, *C*, *D*, *E* and *F* were generated by crystallographic symmetry from protomer *A*. Protomers that form two active sites at the interface are shown in similar colors (*AB*, *CD* and *EF*). Adenosine and sulfate are shown in red in stick representation.

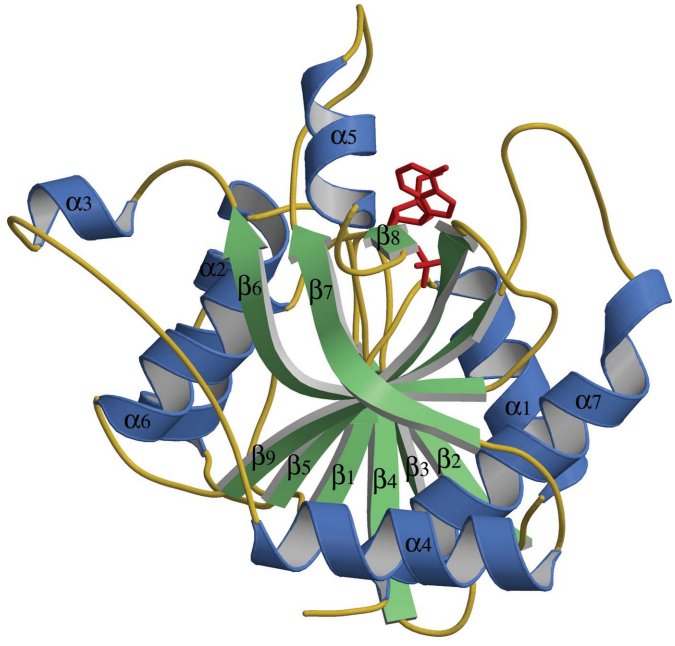

Figure 2
Structure of the *B. cereus* AdoP protomer. The protomer of AdoP is shown in ribbon representation and colored by secondary structure. Adenosine and sulfate are shown in red stick representation.

face of the pentose ring and forms a hydrogen bond to the 2′-hydroxyl group of the ribose. Glu181 makes hydrogen bonds to both hydroxyl groups of the ribose.

Several hydrophobic residues surround the purine ring in the base-binding site, with Val178 and Ile206 on one side and Phe159 and Met180 on the other (Fig. 3). Different interactions between the purine base and Asp204 or Asn204 were detected in the four ternary complexes in which both nucleoside and sulfate are bound in the active site. These different interactions resulted from changes in the position and orientation of Asp204 or Asn204, while the orientation in the active site of the nucleoside was same in all four complexes (Fig. 4). For the AdoP–Ado–SO_4 complex (Fig. 5*a*), Asp204 interacts directly with the base, making two hydrogen bonds to the N7 and N6 atoms of the adenine base. Asp204 also accepts one hydrogen bond from Ser203 and one from a water molecule. A series of water molecules form a hydrogen-bonding network with the N1 and N6 of the base and the carbonyl group of Phe159. In the AdoP–Ino–SO_4 complex (Fig. 5*b*) the Asp204 side chain is positioned further from the base, allowing two well ordered water molecules to bridge between Asp204 and the base. The position of Asn204 in the D204N–Ado–SO_4 complex (Fig. 5*c*) is very similar to the position of Asp204 in the AdoP–Ado–SO_4 complex, with two hydrogen bonds formed between Asn204 and the purine base. In the D204N–Ino–SO_4 complex (Fig. 5*d*), the carboxamido group of Asn204 forms a weak hydrogen bond (∼3.47 Å) to N7 of the purine base and interacts with O6 of the purine base indirectly through a water molecule, as seen in the AdoP–Ino–SO_4 complex. Another feature in common between the two complexes is the network of water molecules that connects N1 and O6 of the purine base and Phe159.

4. Discussion

4.1. Structural basis of substrate specificity

The kinetic parameters reported in Table 3 demonstrate the high specificity of *B. cereus* AdoP for adenosine. A comparison of the interactions between Asp204 and the purine base in the AdoP–Ado–SO_4 and AdoP–Ino–SO_4 ternary complexes may explain the structural basis of its substrate preference. When adenosine is bound in the active site (Fig. 5*a*), the Asp204 side chain is ∼2.76 Å away from the N7 atom of adenosine and is properly oriented to act as a proton donor and offset the partial negative charge that is transferred to the N7 position of the base from the weakening glycosidic bond (Fig. 6). Protonation of the nucleobase in the transition state is essential for leaving-group activation by a mechanism that is analogous to that of human purine nucleoside phosphorylase (Erion, Stoeckler *et al.*, 1997; Kline & Schramm, 1993; Schramm, 1999).

In the active site of the AdoP–Ino–SO_4 complex (Fig. 5*b*), Asp204 interacts indirectly with the base owing to the insertion of two water molecules. In this case, a water molecule could serve as the proton donor to N7 of the purine base, but would be less efficient compared with an acidic amino-acid side chain. Alternatively, AdoP could utilize a mechanism similar to that described for the trimeric PNP from *Cellulomonas* for stabilizing the transition state, involving the delocalization of the electron density on the six-membered

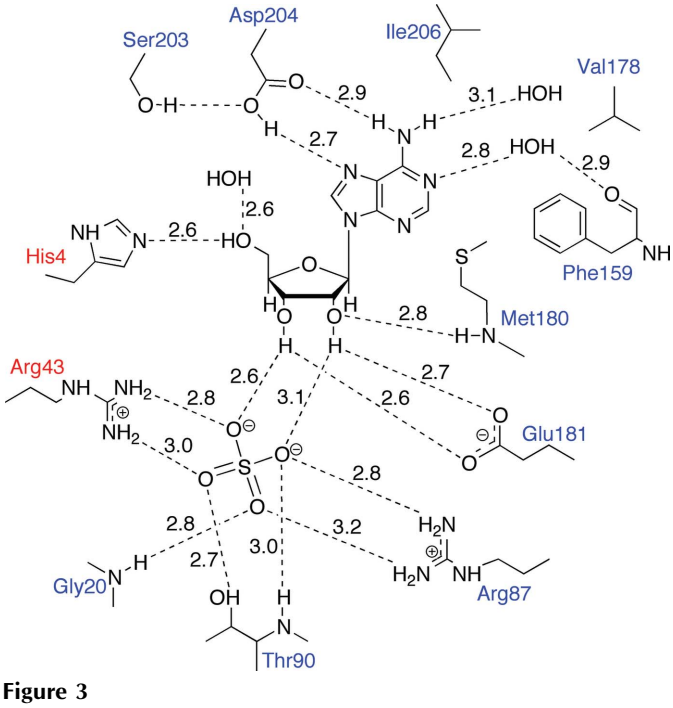

Figure 3
Schematic diagram of the *B. cereus* AdoP active site. Residues belonging to the adjacent subunit are shown in red. Hydrogen bonds are indicated by dashed lines and labeled with donor-to-acceptor distances.

Figure 4
Comparison of Asp204/Asn204 in the four ternary complexes and the AdoP–SO_4 complex. The five structures are superimposed on the basis of secondary-structure element alignment. Color coding is red, AdoP–Ado–SO_4; orange, D204N–Ado–SO_4; blue, D204N–Ino–SO_4; green, AdoP–Ino–SO_4; cyan, AdoP–SO_4.

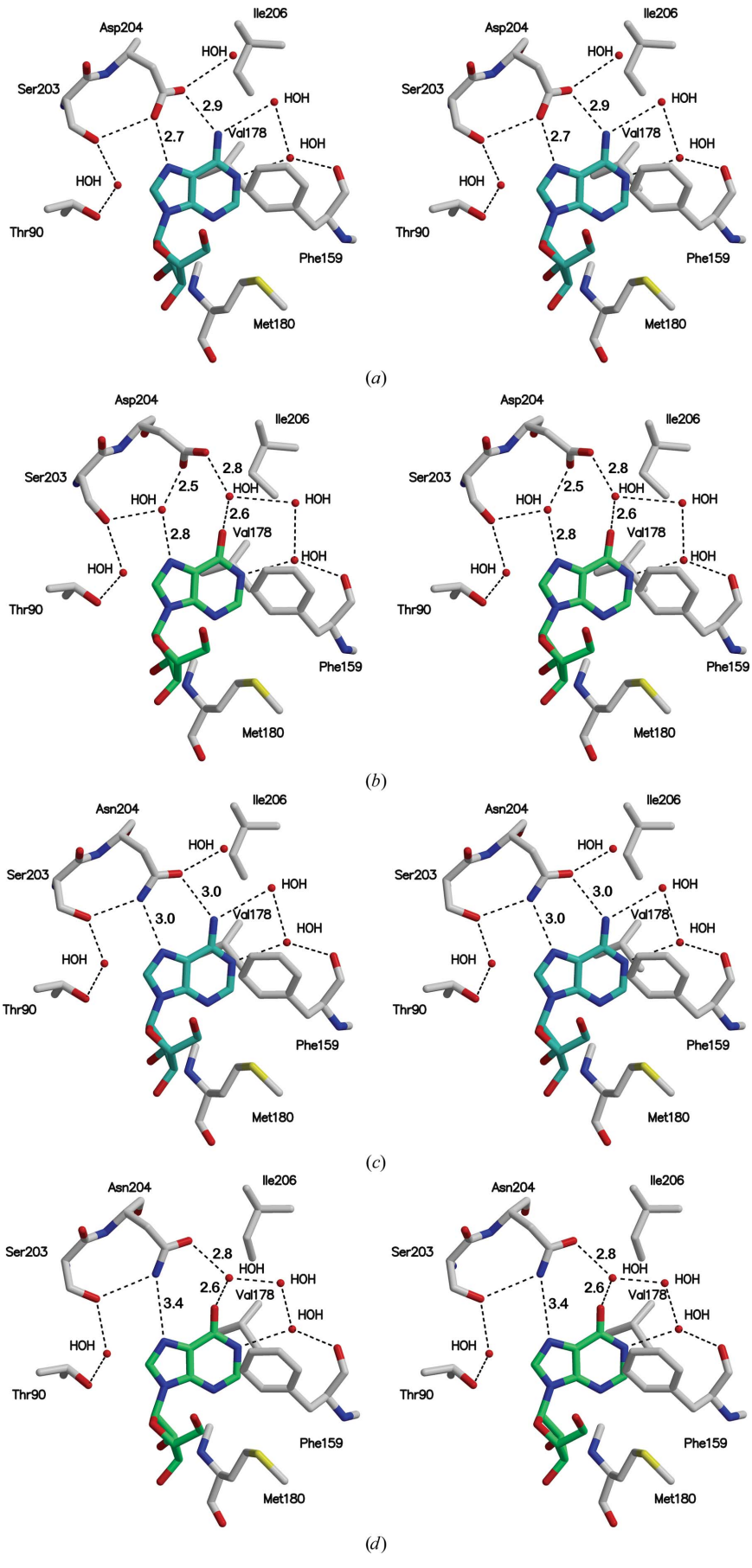

ring of inosine (Tebbe *et al.*, 1999). In the ternary complex of *Cellulomonas* PNP with 8-iodoguanine and phosphate, the negative charge is localized at O6 of the purine base, thus forming an enolate-ion intermediate. The enolic tautomer could be stabilized by a Glu residue (Glu204), which accepts a hydrogen bond from N1 of the purine base. This Glu residue, which is structurally and functionally conserved in human PNP (Glu201) and 5′-deoxy-5′-methylthioadenosine phosphorylase (MTAP) from *Sulfolobus solfataricus* (Glu163), is located outside the active site in *B. cereus* AdoP (Glu162). Mutagenesis studies confirmed that Glu162 does not interact with the substrate (unpublished results). In the structure of the AdoP–Ino–SO_4 complex, an ordered water molecule was found to make a hydrogen bond to N1 and could help to delocalize the electron density in a circuit that involves N1, three water molecules and O6 (Fig. 5*b*). The strength of an N1–water hydrogen bond, however, is less than that of the strong hydrogen bond formed between N1 and Glu201 in human PNP, Glu204 in *Cellulomonas* PNP or Glu163 in *S. solfataricus* MTAP. Compared with the direct interaction of Asp204 and N7, utilizing these two alternative but less efficient ways of stabilizing the transition state could be the molecular basis for the 107-fold preference for adenosine compared with inosine.

4.2. Change in substrate preference of *B. cereus* AdoP

Extensive studies conducted on human PNP have already revealed the importance of the conserved asparagine residue in trimeric PNPs for 6-oxopurine substrate specificity. The N243A mutant led to a 1000-fold decrease in k_{cat} for inosine (Erion, Takabayashi *et al.*, 1997). The cleavage of adenosine by wild-type human PNP is

Figure 5
Stereo diagrams of the base-binding site. (*a*) AdoP–Ado–SO_4 complex. (*b*) AdoP–Ino–SO_4 complex. (*c*) D204N–Ado–SO_4 complex. (*d*) D204N–Ino–SO_4 complex. C atoms are shown in gray for the protein, in light blue for adenosine and in green for inosine. N atoms are shown in blue, O atoms in red and S atoms in yellow. Water molecules are shown as red spheres and labeled HOH. Hydrogen bonds are indicated by dashed lines and labeled with distances in Å.

essentially undetectable, while 6-aminopurine nucleosides were very good substrates for the N243D mutant and were preferred over inosine, thus reversing the substrate specificity (Stoeckler *et al.*, 1997). In addition, PNP from *T. thermophilus*, despite its hexameric quaternary structure normally associated with broad substrate specificity, has an asparagine residue near N7 and its selectivity for inosine is similar to that of the trimeric PNPs (Tahirov *et al.*, 2004).

Two different mechanisms have been proposed for trimeric PNPs on the basis of key catalytic residues. Erion, Stoeckler *et al.* (1997) suggested a role for Asn243 in stabilizing the transition state by donating a hydrogen bond to N, while Tebbe *et al.* (1999) proposed that Asn243 (Asn246 in *Cellulomonas* PNP) supports substrate binding rather than catalysis and that Glu201 (Glu204 in *Cellulomonas* PNP) interacts as the key catalytic residue, as discussed in §4.1.

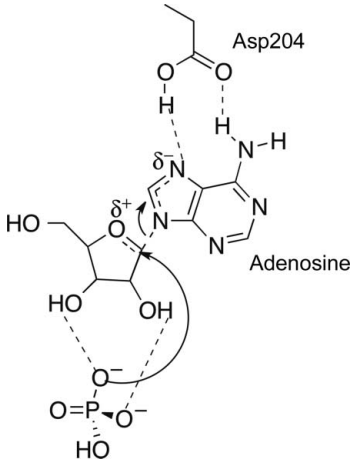

Figure 6
Expected transition state for the phosphorolysis of adenosine by *B. cereus* AdoP.

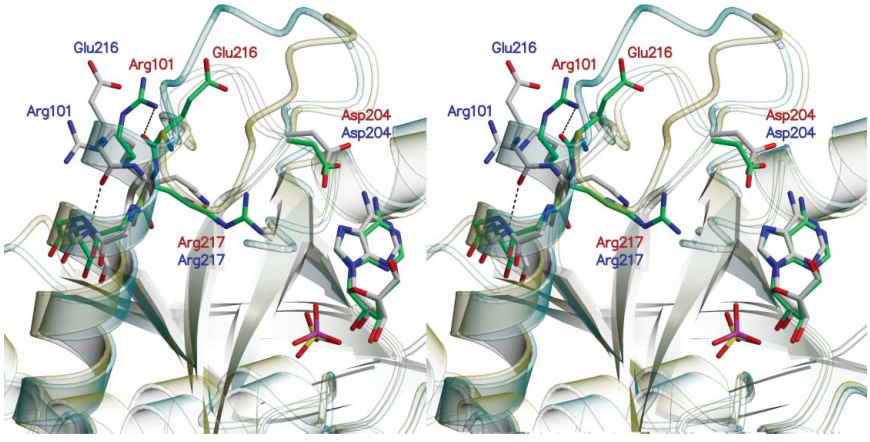

Figure 7
Active-site stereoview of the AdoP–Ado–SO_4 and the *E. coli* PNP–Ado–PO_4 (PDB entry 1pk7; Bennett *et al.*, 2003) complexes superimposed. Secondary structures are shown in ribbon representation and are colored yellow for *B. cereus* AdoP and light blue for *E. coli* PNP. C atoms are shown in green for *B. cereus* AdoP and in gray for *E. coli* PNP. N atoms are shown in blue, O atoms in red, S atoms in yellow and P atoms in magenta. Key residues are shown in stick representation and labeled in red for *B. cereus* AdoP and in blue for *E. coli* PNP. Hydrogen bonds are indicated by dashed lines.

In our studies, mutation of Asp204 to asparagine in *B. cereus* AdoP resulted in a 430-fold decrease in the catalytic efficiency of adenosine cleavage. More significantly, the mutation resulted in no change in the efficiency of inosine cleavage, effectively reversing the substrate specificity. However, N204D only slightly prefers inosine, while wild-type *B. cereus* AdoP strongly prefers adenosine. This result is consistent with the role of asparagine in conferring selectivity towards 6-oxopurines and is complementary to the reversal of substrate specificity obtained with the N243D mutant of human PNP by Stoeckler *et al.* (1997). The structure of the D204N–Ino–SO_4 complex (Fig. 5*d*) provides some insights. In this complex, the distance between the carboxamide group of Asn204 and N7 of the purine base (∼3.47 Å) is not favorable for hydrogen-bond formation. The negative charge on the purine base formed during the transition state could be alternatively delocalized on the six-membered ring of the base and on the network of water molecules that connect N1 and O6 of the purine base, as hypothesized for the AdoP–Ino–SO_4 complex. Consistent with this assumption is the nearly identical k_{cat} of the wild-type enzyme and the D204N mutant towards inosine.

4.3. Comparison between *E. coli* PNP and *B. cereus* AdoP active sites

Among the structurally characterized PNPs, *B. cereus* AdoP, which is 100% identical to *B. anthracis* AdoP, shares the highest sequence identity (56%) with *E. coli* PNP. AdoP strongly prefers adenosine, while *E. coli* PNP has a similar catalytic efficiency for both adenosine and inosine (Bennett *et al.*, 2003). Furthermore, AdoP cleaves adenosine 44-fold more efficiently than *E. coli* PNP. Despite their catalytic differences, the two enzymes exhibit significant similarities in overall structure as well as active-site composition and substrate-binding geometry. Superposition of *B. cereus* AdoP and *E. coli* PNP using *DALI* (Holm & Sander, 1998) showed a root-mean-square deviation of 1.4 Å for 234 aligned residues. The superposition also revealed that 11 of the 12 active-site residues are identical. The exception is Thr90 in the phosphate-binding site of *B. cereus* AdoP, which is replaced by a functionally equivalent Ser90 in *E. coli* PNP.

A superimposition of the active sites of the two enzymes each complexed with adenosine and sulfate is shown in Fig. 7. The major difference between the two binding sites is the conformation of the loop region from residues 207 to 217. Compared with *E. coli* PNP, loop 207–217 in *B. cereus* AdoP adopts a more closed conformation. This different positioning of loop 207–217 appears to compensate for a disruption of the N-terminal end of helix α_7 in *B. cereus* AdoP caused by a different orientation of the Arg217 side chain with respect to the equivalent residue in *E. coli* PNP. As a

result, in *B. cereus* AdoP the backbone carbonyl of Glu216 is prevented from making a hydrogen bond to the backbone amide of Thr220 and contributing to the first turn of helix α_7, as in the case of *E. coli* PNP. Instead, Glu216 is involved in a hydrogen bond to the side chain of Arg101 from the loop connecting β_5 and β_6 (Fig. 7). In all *B. cereus* AdoP complex structures, loop 207–217 is either partially disordered or has relatively high *B* factors, suggesting that this loop could be flexible during substrate binding and product release. The same region also showed different conformations from protomer to protomer in *E. coli* PNP complexes; there are three crystallographically independent protomers in the structure (Bennett *et al.*, 2003).

Comparison of *B. cereus* AdoP with *E. coli* PNP suggests that it would be difficult to predict *a priori* the relative substrate specificities of these two types of nucleoside phosphorylases. One possibility is that the high efficiency of *B. cereus* AdoP for adenosine compared with *E. coli* PNP could be the result of a less open active site and better positioning and orientation of the catalytically important aspartic acid residue with respect to adenosine. An Asp204 to asparagine mutant has recently been reported for *E. coli* PNP; however, no structural data were reported for the mutants or their complexes (Mikleušević *et al.*, 2011). Relative activities at fixed substrate concentrations showed significant reductions of activity towards adenosine, inosine and guanosine of approximately 800-fold, 70-fold and 30-fold, respectively. Detailed structural and kinetic studies are needed to further assess the role of residue 204 in the determination of substrate specificity for *E. coli* PNP.

5. Conclusion

The biochemical and kinetic studies reported here show that Asp204 plays an important role in the preference of *B. cereus* AdoP for adenosine. Mutation of Asp204 to asparagine results in a significant decrease in the efficiency of adenosine cleavage and a slight increase in the efficiency of inosine cleavage, thus resulting in a reversal of substrate preference. The structural data correlate with the kinetic results and suggest that AdoP and its mutants can stabilize the transition state in various ways but that these are not equally favored energetically. The most favorable geometry occurs when adenosine is bound in the active site, with Asp204 directly protonating the adenine at N7.

This work was supported by funding from the University of Sassari, Italy (FS) and by National Institutes of Health grant GM073220 (SEE). This work is based upon research conducted at the Advanced Photon Source on the Northeastern Collaborative Access Team beamlines, which are supported by award RR-15301 from the National Center for Research Resources at the National Institutes of Health. Use of the Advanced Photon Source is supported by the US Department of Energy, Office of Basic Energy Sciences under Contract No. DE-AC02-06CH11357.

References

Adams, P. D. *et al.* (2011). *Methods*, **55**, 94–106.
Allegrini, S., Pesi, R., Tozzi, M. G., Fiol, C. J., Johnson, R. B. & Eriksson, S. (1997). *Biochem. J.* **328**, 483–487.
Appleby, T. C., Mathews, I. I., Porcelli, M., Cacciapuoti, G. & Ealick, S. E. (2001). *J. Biol. Chem.* **276**, 39232–39242.
Atlas, R. M. (1998). *Crit. Rev. Microbiol.* **24**, 157–168.
Bennett, E. M., Li, C., Allan, P. W., Parker, W. B. & Ealick, S. E. (2003). *J. Biol. Chem.* **278**, 47110–47118.
Bradford, M. M. (1976). *Anal. Biochem.* **72**, 248–254.
Brünger, A. T., Adams, P. D., Clore, G. M., DeLano, W. L., Gros, P., Grosse-Kunstleve, R. W., Jiang, J.-S., Kuszewski, J., Nilges, M., Pannu, N. S., Read, R. J., Rice, L. M., Simonson, T. & Warren, G. L. (1998). *Acta Cryst.* D**54**, 905–921.
Bzowska, A., Kulikowska, E. & Shugar, D. (2000). *Pharmacol. Ther.* **88**, 349–425.
Daddona, P. E., Wiesmann, W. P., Milhouse, W., Chern, J. W., Townsend, L. B., Hershfield, M. S. & Webster, H. K. (1986). *J. Biol. Chem.* **261**, 11667–11673.
DeLano, W. L. (2002). *PyMOL*. http://www.pymol.org.
Ekici, A. B., Park, O. S., Fuchs, C. & Rautenstrauss, B. (1997). *Tech. Tips Online*, **2**, 121–123.
Emsley, P., Lohkamp, B., Scott, W. G. & Cowtan, K. (2010). *Acta Cryst.* D**66**, 486–501.
Erion, M. D., Stoeckler, J. D., Guida, W. C., Walter, R. L. & Ealick, S. E. (1997). *Biochemistry*, **36**, 11735–11748.
Erion, M. D., Takabayashi, K., Smith, H. B., Kessi, J., Wagner, S., Hönger, S., Shames, S. L. & Ealick, S. E. (1997). *Biochemistry*, **36**, 11725–11734.
Gardner, R. & Kornberg, A. (1967). *J. Biol. Chem.* **242**, 2383–2388.
Grenha, R., Levdikov, V. M., Fogg, M. J., Blagova, E. V., Brannigan, J. A., Wilkinson, A. J. & Wilson, K. S. (2005). *Acta Cryst.* F**61**, 459–462.
Holm, L. & Sander, C. (1998). *Nucleic Acids Res.* **26**, 316–319.
Ivanova, N. *et al.* (2003). *Nature (London)*, **423**, 87–91.
Jensen, K. F. (1978). *Biochim. Biophys. Acta*, **525**, 346–356.
Jones, T. A., Zou, J.-Y., Cowan, S. W. & Kjeldgaard, M. (1991). *Acta Cryst.* A**47**, 110–119.
Kalckar, H. M. (1947). *J. Biol. Chem.* **167**, 477–486.
Kline, P. C. & Schramm, V. L. (1993). *Biochemistry*, **32**, 13212–13219.
Kraulis, P. J. (1991). *J. Appl. Cryst.* **24**, 946–950.
Mao, C., Cook, W. J., Zhou, M., Koszalka, G. W., Krenitsky, T. A. & Ealick, S. E. (1997). *Structure*, **5**, 1373–1383.
Matthews, B. W. (1968). *J. Mol. Biol.* **33**, 491–497.
McElwain, M. C., Williams, M. V. & Pollack, J. D. (1988). *J. Bacteriol.* **170**, 564–567.
Merritt, E. A. & Bacon, D. J. (1997). *Methods Enzymol.* **277**, 505–524.
Miech, F. P., Senft, A. W. & Senft, D. G. (1975). *Biochem. Pharmacol.* **24**, 407–411.
Mikleušević, G., Stefanić, Z., Narczyk, M., Wielgus-Kutrowska, B., Bzowska, A. & Luić, M. (2011). *Biochimie*, **93**, 1610–1622.
Otwinowski, Z. & Minor, W. (1997). *Methods Enzymol.* **276**, 307–326.
Pugmire, M. J. & Ealick, S. E. (2002). *Biochem. J.* **361**, 1–25.
Read, T. D. *et al.* (2003). *Nature (London)*, **423**, 81–86.
Schnick, C., Robien, M. A., Brzozowski, A. M., Dodson, E. J., Murshudov, G. N., Anderson, L., Luft, J. R., Mehlin, C., Hol, W. G. J., Brannigan, J. A. & Wilkinson, A. J. (2005). *Acta Cryst.* D**61**, 1245–1254.
Schramm, V. L. (1999). *Methods Enzymol.* **308**, 301–355.
Scopes, R. K. (1974). *Anal. Biochem.* **59**, 277–282.
Senesi, S., Falcone, G., Mura, U., Sgarrella, F. & Ipata, P. L. (1976). *FEBS Lett.* **64**, 353–357.
Senesi, S., Falcone, G., Mura, U., Sgarrella, F. & Ipata, P. L. (1977). *Spore Research 1976*, Vol. 1, edited by A. N. Barker, J. Wolf, D. J. Ellar, G. J. Dring & G. W. Gould, pp. 311–333. London: Academic Press.

Sgarrella, F., Frassetto, L., Allegrini, S., Camici, M., Carta, M. C., Fadda, P., Tozzi, M. G. & Ipata, P. L. (2007). *Biochim. Biophys. Acta*, **1770**, 1498–1505.
Shi, W., Ting, L.-M., Kicska, G. A., Lewandowicz, A., Tyler, P. C., Evans, G. B., Furneaux, R. H., Kim, K., Almo, S. C. & Schramm, V. L. (2004). *J. Biol. Chem.* **279**, 18103–18106.
Stoeckler, J. D., Poirot, A. F., Smith, R. M., Parks, R. E., Ealick, S. E., Takabayashi, K. & Erion, M. D. (1997). *Biochemistry*, **36**, 11749–11756.
Tahirov, T. H., Inagaki, E., Ohshima, N., Kitao, T., Kuroishi, C., Ukita, Y., Takio, K., Kobayashi, M., Kuramitsu, S., Yokoyama, S. & Miyano, M. (2004). *J. Mol. Biol.* **337**, 1149–1160.
Tebbe, J., Bzowska, A., Wielgus-Kutrowska, B., Schröder, W., Kazimierczuk, Z., Shugar, D., Saenger, W. & Koellner, G. (1999). *J. Mol. Biol.* **294**, 1239–1255.
Tozzi, M. G., Camici, M., Mascia, L., Sgarrella, F. & Ipata, P. L. (2006). *FEBS J.* **273**, 1089–1101.
Tozzi, M. G., Sgarrella, F. & Ipata, P. L. (1981). *Biochim. Biophys. Acta*, **678**, 460–466.
Trembacz, H. & Jezewska, M. M. (1993). *Comp. Biochem. Physiol. B*, **104**, 481–487.
Trembacz, H. & Jezewska, M. M. (1998). *Adv. Exp. Med. Biol.* **431**, 711–717.
Zang, Y., Wang, W.-H., Wu, S.-W., Ealick, S. E. & Wang, C. C. (2005). *J. Biol. Chem.* **280**, 22318–22325.
Zwart, P. H., Grosse-Kunstleve, R. W. & Adams, P. D. (2005*a*). *CCP4 Newsl.* **42**, 58–67.
Zwart, P. H., Grosse-Kunstleve, R. W. & Adams, P. D. (2005*b*). *CCP4 Newsl.* **43**, 26–35.